Biosensors and Bioelectronics 78 (2016) 92–99

Contents lists available at ScienceDirect

Biosensors and Bioelectronics

journal homepage: www.elsevier.com/locate/bios

Acoustic wave biosensor for the detection of the breast and prostate cancer metastasis biomarker protein PTHrP

Victor Crivianu-Gaita [a], Mohamed Aamer [a], Roy T. Posaratnanathan [a], Alexander Romaschin [b], Michael Thompson [a,*]

[a] Department of Chemistry, University of Toronto, Toronto, ON, Canada M5S 3H6
[b] Clinical Biochemistry, St. Michael's Hospital, Toronto, ON, Canada M5B 1W8

ARTICLE INFO

Article history:
Received 23 September 2015
Received in revised form
2 November 2015
Accepted 10 November 2015
Available online 12 November 2015

Keywords:
Acoustic wave sensor
Parathyroid hormone-related peptide
Fab' fragments
Antibodies
Biosensor
Cancer metastasis

ABSTRACT

There are currently no biosensors that are able to reliably detect the process of cancer metastasis. We describe the first label-free real-time ultra-high frequency acoustic wave biosensor prototype capable of detecting the breast and prostate cancer metastasis biomarker, parathyroid hormone-related peptide (PTHrP). Two different linkers – 11-trichlorosilyl-undecanoic acid pentafluorophenyl ester (PFP) and S-(11-trichlorosilyl-undecanyl)-benzothiosulfonate (TUBTS) – were used to immobilize whole anti-PTHrP antibodies and Fab' fragments to surfaces as biorecognition elements. The biosensor surfaces were optimized using X-ray photoelectron spectroscopy (XPS) and the ultra-high frequency electromagnetic piezoelectric acoustic sensor (EMPAS). One optimized whole antibody-based surface (PFP/protein G'/whole antibodies/ethanolamine) and one optimized Fab' fragment-based surface (TUBTS/Fab' fragments) were tested as biosensors. It was determined that an in-line injection of bovine serum albumin prior to analyte injection yielded the most minimally fouling surfaces. Each surface was tested with no mass amplification and with sandwich-type secondary antibody mass amplification. The whole antibody-based mass-amplified biosensor yielded the lowest limit of detection (61 ng/mL), highest sensitivity, and a linear range from 61 ng/mL to 100 μg/mL. However, the Fab' fragment-based biosensor displayed better regenerability as a loss of ~20% of the initial analyte signal intensity was observed with each subsequent injection. The whole antibody-based biosensor was only capable of producing an analyte signal in the first injection.

1. Introduction

Malignant breast cancer is the most common neoplastic disease affecting women in the Western world (Weigelt et al., 2005). For males, prostate cancer was the third leading cause of death from cancer in 2012 (Morisot et al., 2015). When a cancer has developed additional tumors at locations different from the initial primary tumor, the process is known metastasis (Geiger and Peeper, 2009; Weber, 2008). Metastatic cancer drastically reduces the patient's chance of survival (Hall et al., 2000; Lyden et al., 2011).

Certain tumors, particularly those showing preferential metastasis to the bone, produce parathyroid-hormone related peptide (PTHrP) (Lyden et al., 2011). PTHrP is involved in the regulation of cartilage growth during bone development in childhood, however, this peptide ceases to have physiological function in adulthood (Mundy and Edwards, 2008). Increased levels of PTHrP have been found in several types of cancer (Fig. 1) (Nakajima et al., 2002). The presence of PTHrP outside of childhood is an indicator of one of two possible scenarios: (1) the PTHrP is causing humoral hypercalcemia of malignancy but is not involved in the metastasis of the cancer (2) the PTHrP is directly involved in the metastatic pathway through the growth and differentiation of neoplastic cells (Guise et al., 1996; Mundy and Edwards, 2008). The latter phenomenon is observed in breast and prostate cancer, where elevated PTHrP levels correlate with the subsequent formation of bone metastases (Nishihara et al., 2007).

Currently, there are no methods to efficiently and reliably detect cancer metastasis. The very few biosensors that have been developed focus on the sequestration and detection of circulating tumor cells (CTCs) (Abdolahad et al., 2012; Bohunicky and Mousa, 2011; Costa et al., 2014). These CTCs are released from the primary tumor into the bloodstream where they can seed in different locations and promote the growth of a secondary tumor (Costa et al., 2014). However, CTCs are not often present in the bloodstream and an attempt to detect them is akin to "finding a needle in a

* Correspondence to: Lash Miller Chemical Laboratories, 80 St. George Street, Toronto, ON, Canada.
E-mail address: mikethom@chem.utoronto.ca (M. Thompson).

http://dx.doi.org/10.1016/j.bios.2015.11.031
0956-5663/

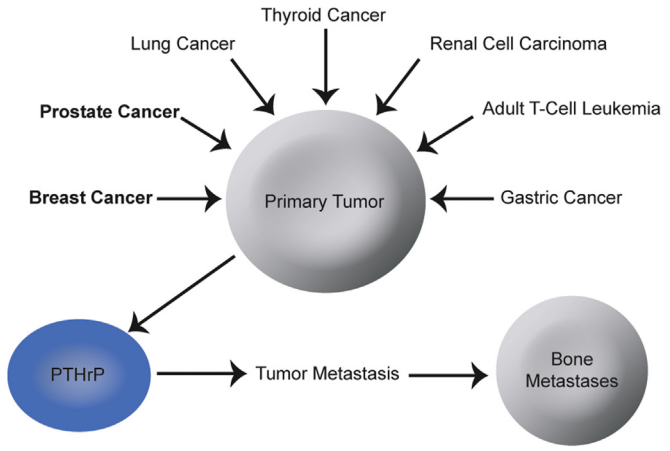

Fig. 1. Elevated levels of PTHrP have been detected in various types of cancers. The presence of this biomarker is an indicator of metastasis of breast and prostate cancers. PTHrP is directly involved in the metastatic pathway of these two cancers resulting in bone metastases.

haystack". Typically, cancer metastasis can only be detected once it has occurred and the affected individual's chance of survival has been significantly decreased. In this article, we present the prototype of the first biosensor capable of detecting cancer metastasis in real-time through the detection of the protein biomarker PTHrP. Unlike CTCs, PTHrP is constantly present in the blood of individuals affected by the various cancers listed in Fig. 1 (Suehiro et al., 1994).

The biosensor prototype designed to detect PTHrP is based on the electromagnetic piezoelectric acoustic device (EMPAS) (Ballantyne and Thompson, 2004). For a more technical diagram of the EMPAS, the reader is advised to look through the study by Thompson et al. (2003). Unlike other bulk acoustic wave (BAW) device, such as the quartz crystal microbalance (QCM), the EMPAS operates as an electrode-free sensor where the piezoelectric quartz disk is stimulated through an external magnetic field, generated by a flat spiral coil beneath the disk (Ballantyne and Thompson, 2004; Thompson et al., 2003). This allows the EMPAS to operate at ultra-high frequencies (>1 GHz) resulting in a significantly higher sensitivity compared to the QCM (Ballantyne and Thompson, 2004). Although a greater amount of noise is associated with higher frequencies, previous experiments in our lab have found that the the signal-to-noise ratio increases at higher frequencies. Compared to surface acoustic wave (SAW) devices where the compressional component of the Rayleigh wave is attenuated in liquid media (Ballantine and Wohltjen, (1989)), the EMPAS offers shear wave propagation through the bulk quartz, allowing for operation in liquid media without significant damping (Kaspar et al., 2000). The frequency tuneability of the EMPAS allows for probing of the sensor's interfacial region at varying depths (Ballantyne and Thompson, 2004). The high frequency operation of the EMPAS allows for a reduction in the penetration depth, therefore removing potential signal interference effects (i.e. viscoelastic slip) produced by the self-assembled monolayers. The device has previously been used in a number of different studies, such as for the detection of HIV-2 antibodies, cocaine, fouling levels of surfaces, and lipopolysaccharide pathogens (Neves et al., 2015; Sheikh et al., 2012, 2011; Thompson et al., 2014).

The surfaces used for the development of the biosensor involve the formation of self-assembled monolayers (SAMs) (Hader et al., 2012; Schreiber, 2000). Compounds that form SAMs consist of three parts – an end-group providing the surface properties of the monolayer, a backbone, and a headgroup used to covalently immobilize onto the surface (Schreiber, 2000). In this study we employ the use of 11-trichlorosilyl-undecanoic acid pentafluorophenyl ester (PFP) and S-(11-trichlorosilyl-undecanyl)-benzothiosulfonate (TUBTS) as the compounds used to form the two different SAMs used in the biosensor development (Blaszykowski et al., 2012).

The first part of the biosensor development involves the optimization of the biosensing surfaces – minimization of undesirable surface fouling and maximization of analyte signal. The second part tests the optimized surfaces as biosensors. The biorecognition elements used in this study are whole antibodies (Ab) and their respective fragment antigen-binding (Fab') units. Antibodies have extremely high specificity towards their target analyte and have been used for decades in the field of biosensing (Bonroy et al., 2006; Viitala et al., 2000; Vikholm-Lundin and Albers, 2006; Vikholm-Lundin, 2005). Whole antibodies-based surfaces and Fab' fragment-based surfaces were then compared as the latter have been found to produce lower limits of detection and higher immobilization densities on the surfaces (Crivianu-Gaita and Thompson, 2015). These Fab' fragments are covalently immobilized to surfaces via their nucleophilic C-terminal sulfides.

The biosensor in this study offers a real-time label-free sensor capable of detecting the cancer metastasis biomarker protein PTHrP. This biosensor is the first step towards the efficient and reliable detection of cancer metastasis.

2. Materials and methods

2.1. Chemicals

The linkers 11-trichlorosilyl-undecanoic acid pentafluorophenyl ester (PFP) and S-(11-trichlorosilyl-undecanyl)-benzothiosulfonate (TUBTS) were prepared according to previous protocols (Blaszykowski et al., 2012). Quartz disks for EMPAS analysis were purchased from Laptech Precision Inc. (Canada) with the following specifications: AT-cut, 0.537 in. in diameter, 20.091 MHz fundamental frequency. Rabbit polyclonal anti-goat IgG antibodies (G5518) and goat IgG (I5256) were purchased from Sigma (Canada). Primary mouse monoclonal anti-PTHrP antibodies (sc-53936) and secondary rabbit polyclonal anti-PTHrP antibodies (sc-20728) were purchased from Santa Cruz (USA). Full length human PTHrP (ab51706) was ordered from Abcam (Canada). Recombinant protein G' (P4689) was purchased from Sigma (Canada). All other chemicals were purchased from Sigma (Canada) and used without further purification.

EMPAS buffer was made to be either pH 7.4 or pH 8.5 with 50 mM sodium phosphate dibasic, 150 mM sodium chloride, and deionized water. Ethanolamine (ETH) buffer was made to have a final concentration of 100 mM ETH in pH 8.5 EMPAS buffer. Cystine (CYS) buffer was made to have a final concentration of 100 mM CYS in pH 8.5 EMPAS buffer.

2.2. Antibody cleavage and Fab' isolation

Primary mouse anti-PTHrP antibodies were pre-treated with PNGase F according to known protocols in order to prepare them for subsequent pepsin cleavage (Wilson et al., 2002). The treated antibodies were then subjected to pepsin (4 h) and dithiothreitol (DTT) (3 h) and separated using a size-exclusion HPLC column according to published protocols (Crivianu-Gaita et al., 2015). A sample of the isolated Fab' fragments were tested using Ellman's reagent to ensure the presence of the nucleophilic C-terminal sulfides (Crivianu-Gaita et al., 2015). Anti-goat IgG antibodies were cleaved according to known protocols (Crivianu-Gaita et al., 2015).

2.3. Quartz disk preparation

Quartz disks were cleaned and prepared according to previous protocols (Sheikh et al., 2012).

2.4. Silanization of the quartz disks

In order to ensure silanization proceeded without problems, the walls of the glassware were pre-silanized in a 1:10 (v/v) mixture with octadecyltrichlorosilane (OTS). Quartz disks were individually transferred to silanized test tubes and moved into a glovebox under nitrogen atmosphere. Linker solutions of PFP and TUBTS were made individually in a ratio of 1 μL linker to 1 mL anhydrous toluene. Portions of 1 mL of the linker solutions were added individually to the test tubes. The tubes were then sealed with rubber stoppers, removed from the glovebox, and allowed to sit on a spin plate for 2 h. The quartz disks were then rinsed three times with toluene, three times with chloroform, and gently dried under a gentle stream of nitrogen before being stored in new scintillation vials.

2.5. Surfaces containing whole antibodies

Quartz disks that were silanized with PFP were used to create surfaces with whole antibodies. Non-oriented whole antibodies were immobilized onto the surfaces by reacting 1 mL aliquots of antibody solutions (20 μg/mL) in pH 7.4 EMPAS buffer with each quartz disk overnight at room temperature. If ETH was used to block the remaining PFP sites on the surfaces, 1 mL aliquots of ETH buffer were reacted with the surfaces for 1 h at room temperature. Surfaces were rinsed three times with pH 7.4 EMPAS buffer and three times with distilled water after each step and before being dried under a gentle nitrogen stream.

To create surfaces containing oriented whole antibodies, recombinant protein G' (50 μg/mL) in pH 7.4 EMPAS buffer was reacted with the PFP surfaces overnight at room temperature (Fig. 2A). If ETH was used to block the remaining PFP sites on the surfaces, 1 mL aliquots of ETH buffer were reacted with the

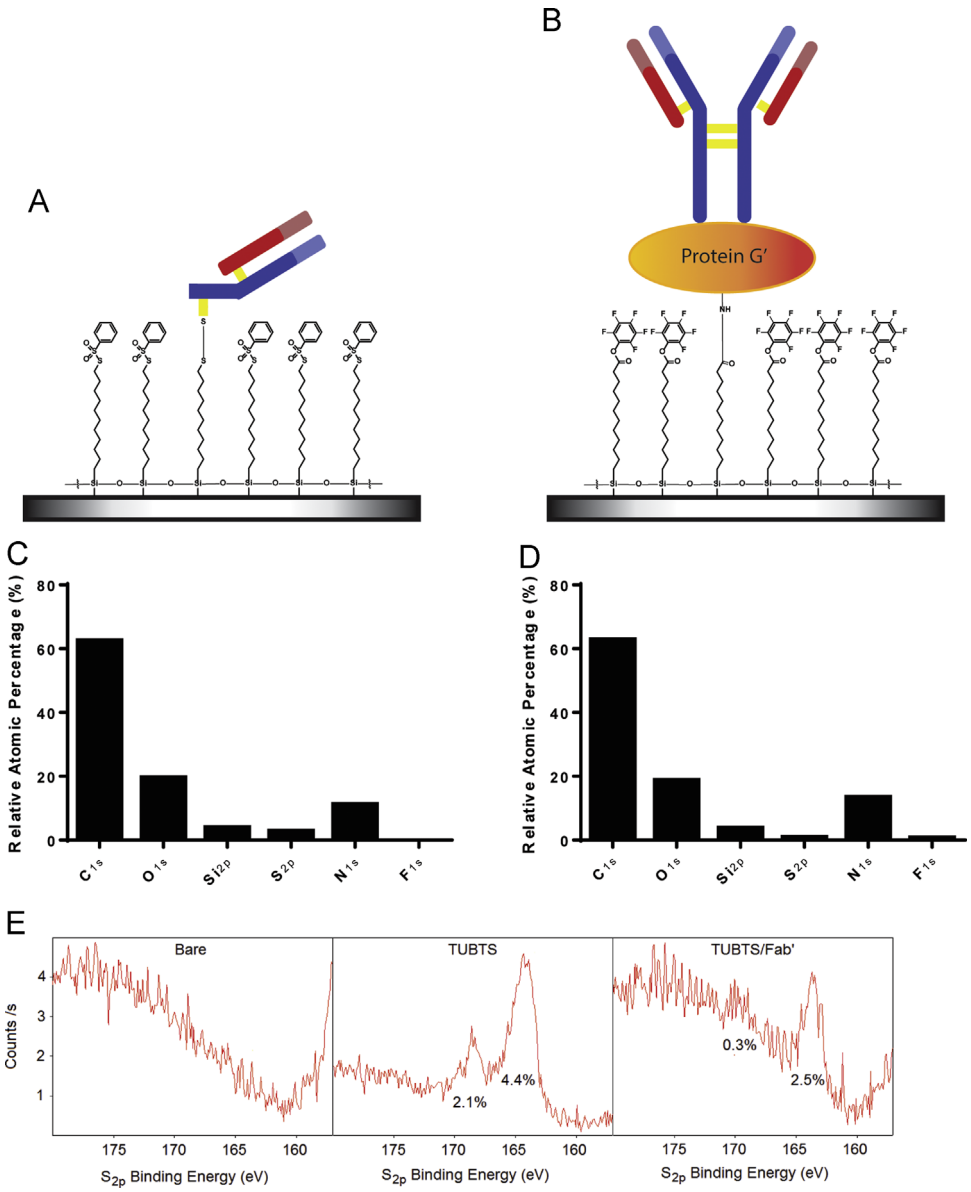

Fig. 2. (A) Illustration of the TUBTS/Fab' surfaces and the orientation of the Fab' fragments. (B) Illustration of the PFP/Oriented Ab surfaces where recombinant protein G' is used to orient whole antibodies. (C) The XPS relative atomic percentages of the TUBTS/Fab' surfaces and the (D) PFP/Oriented Ab surfaces. (E) S_{2p} XPS signals illustrating the decrease of the sulfone (169 ev)/sulfide (164 eV) peak ratios upon Fab' fragment binding.

surfaces for 1 h at room temperature. Aliquots of 1 mL of antibody solutions (20 μg/mL) in pH 7.4 EMPAS buffer were then allowed to react with the surfaces overnight at room temperature. Surfaces were rinsed three times with pH 7.4 EMPAS buffer and three times with distilled water after each step and before being dried under a gentle nitrogen stream.

2.6. Surfaces containing Fab' fragments

Quartz disks that were silanized with PFP were used to create surfaces with non-oriented Fab' fragments. PFP surfaces were reacted with 1 mL aliquots of Fab' fragments (20 μg/mL) in pH 7.4 EMPAS buffer overnight at room temperature. If ETH was used to block the remaining PFP sites on the surfaces, 1 mL aliquots of ETH buffer were reacted with the surfaces for 1 h at room temperature. Surfaces were rinsed three times with pH 7.4 EMPAS buffer and three times with distilled water after each step and before being dried under a gentle nitrogen stream.

Quartz disks that were silanized with TUBTS were used to create surfaces with oriented Fab' fragments (Fig. 2B). TUBTS surfaces were reacted with 1 mL aliquots of Fab' fragments (20 μg/mL) in pH 7.4 EMPAS buffer overnight at room temperature. If CYS was used to block the remaining TUBTS sites on the surfaces, 1 mL aliquots of CYS buffer were reacted with the surfaces for 1 h at room temperature. Surfaces were rinsed three times with pH 7.4 EMPAS buffer and three times with distilled water after each step and before being dried under a gentle nitrogen stream.

2.7. Surface characterization using X-ray photoelectron spectroscopy (XPS)

XPS was used to confirm the various different surfaces created (Fig. 2C, D, Supp Info) as well as to illustrate the binding mechanism of the Fab' fragments onto the TUBTS surfaces (Fig. 2E). Angle-resolved analyses were performed at *Surface Interface Ontario* (Canada) with a Theta probe ThermoFisher Scientific Instrument (UK). A 20° take-off angle relative to the normal was used with Al Kα X-rays. Peaks were calibrated to the C_{1s} signal at 285 eV and the *Avantage* software was used for peak fitting and data analysis. Complete XPS data are available in the Supplementary information file.

2.8. EMPAS measurements

The EMPAS system was setup according to previous protocols (Ballantyne and Thompson, 2004) and each point was measured in triplicate. The quartz disks to be analyzed were loaded into the sample holder and pH 7.4 EMPAS buffer was flowed through constantly at a rate of 50 μL/min. Measurements were performed at the ultra-high frequency of 1.02 GHz (51st harmonic). The

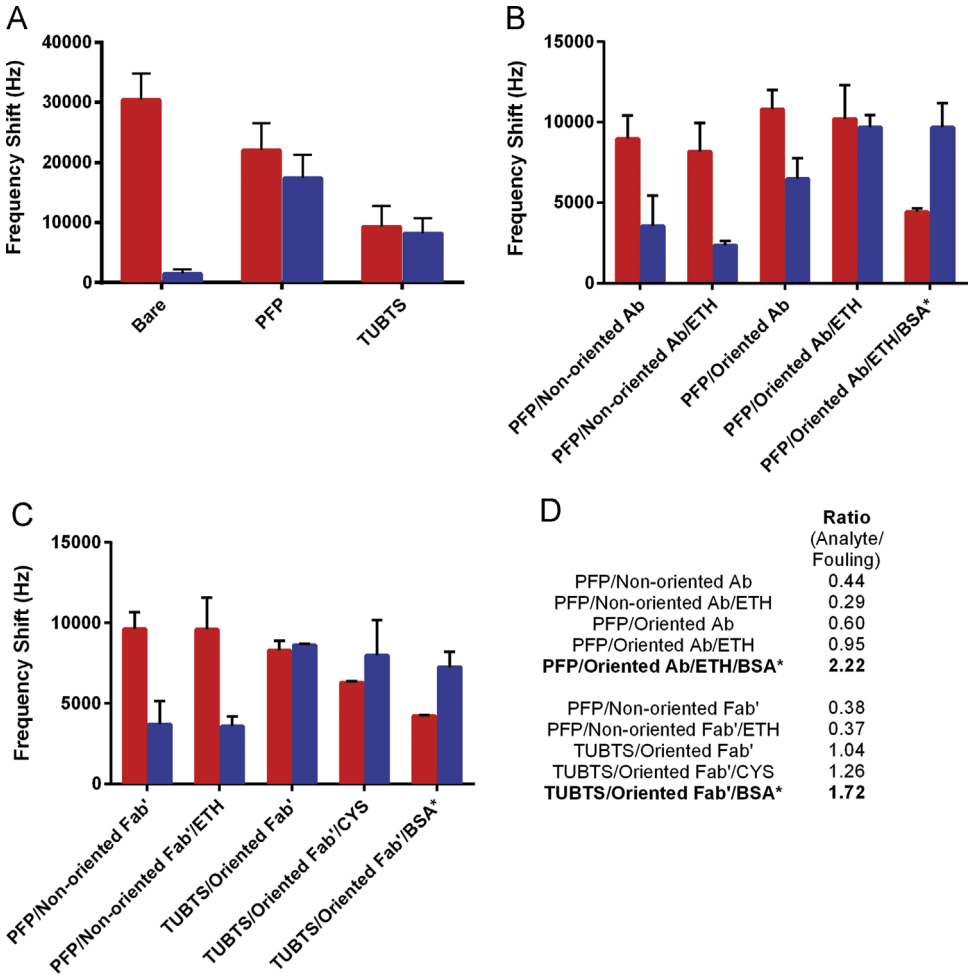

Fig. 3. Red – mouse serum fouling signal. Blue – goat IgG (0.1 mg/mL in pH 7.4 EMPAS buffer) analyte signal. (A) – the fouling levels of bare quartz, PFP-covered, and TUBTS-covered disks. (B) – the fouling and analyte signals for the surfaces tested involving whole antibodies. (C) – the fouling and analyte signals for the surfaces tested involving Fab' fragments. (D) – assessment of all of the surfaces through the ratio of analyte signal/fouling signal. *Bovine serum albumin (BSA) (1 mg/mL in pH 7.4 EMPAS buffer) was injected prior to the sample injection as an anti-fouling agent. (For interpretation of the references to color in this figure legend, the reader is referred to the web version of this article.)

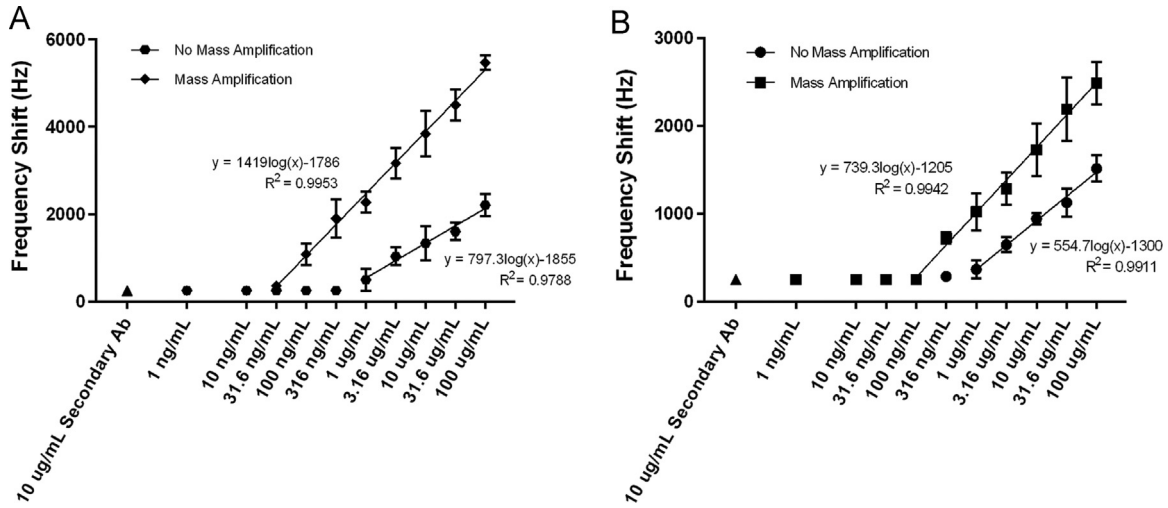

Fig. 4. (A) Comparison of non-mass amplified and mass-amplified PFP/Oriented Ab/ETH/BSA* surfaces. (B) Comparison of non-mass amplified and mass-amplified TUBTS/Fab'/BSA* surfaces. *Bovine serum albumin (BSA) (1 mg/mL in pH 7.4 EMPAS buffer) was injected prior to the sample injection as an anti-fouling agent.

frequency shift was measured as the difference between the stabilized pre-injection signal and the stabilized post-injection signal. In the optimization part of this study, fouling levels of the surfaces were measured using mouse serum and anti-goat IgG antibodies were used to detect the goat IgG analyte (0.1 mg/mL in pH 7.4 EMPAS buffer). Due to the extremely costly nature of the anti-PTHrP antibodies, these antibodies were only used once the surfaces were optimized and ready to be tested as biosensors. Complete EMPAS frequency shifts for Fig. 3 and Fig. 4 are shown in the Supplementary information file.

2.9. Calculation of limit of detection

The software program *GraphPad Prism 6.0* was used for the least squares non-linear regression analysis of the calibration curves as well as for the generation of any of the graphs illustrated in the upcoming figures. The limit of detection (C_{LoD}) was determined using the slope and intercept calculated from the non-linear regressions as well as the blank noise of the EMPAS instrument. According to Eq. (1), S_{EMPAS} represents the blank noise of the EMPAS sensor, determined to be 250 Hz (Ballantyne and Thompson, 2004), m is the slope of the non-linear regression line, and b is the y-intercept of the calculated non-linear regression line.

$$C_{LoD} = 10^{\{[(3*S_{EMPAS})-b]/m\}} \quad (1)$$

3. Results and discussion

3.1. TUBTS-based surfaces and Fab' fragment binding

The surfaces created in this study were analyzed and confirmed using XPS. Bare quartz disks containing surface hydroxyls exhibited only C_{1s}, O_{1s}, and Si_{2p} signals. It should be noted that adventitious carbon is an unavoidable component of all of the XPS analyses and will increase the C_{1s} signals. Immobilization of SAMs of TUBTS onto the quartz disks were detected by an increase in the S_{2p} signal – from 0.0% for bare quartz to 6.5% for TUBTS covered disks. The TUBTS structure contains two different types of sulfur atoms – a sulfide and a sulfone. The former is found at a binding energy of 164 eV whereas the latter is at 169 eV (Fig. 2E). Furthermore, a decrease in the Si_{2p} signal upon TUBTS binding is indicative of the formation of a layer on top of the bulk quartz substrate.

Oriented Fab' fragment binding to the TUBTS occurs through the nucleophilic C-terminal sulfides on the fragment (Fig. 2A). TUBTS has been demonstrated to react in a highly specific manner with sulfides (Benvenuto et al., 2015; Neves et al., 2015). Rabbit IgG polyclonal antibodies and mouse IgG1 monoclonal antibodies yield Fab' fragments containing ~1 and ~4 nucleophilic C-terminal sulfides, respectively (Crivianu-gaita et al., 2015; Liu and May, 2012). The results of Ellman's test with the antibodies used in this study produced values between 0.88 and 0.96 sulfides per Fab' fragment for rabbit polyclonal antibodies. For mouse monoclonal antibodies the values were between 3.79 and 4.04 sulfides per Fab' fragment. This shows that the only reactive sulfides on the Fab' fragments are on the C-terminals of the fragments. The C-terminals of the Fab' fragments originate from the hinge region of the antibody, which has been shown to not be in a globular domain of the antibody (Adlersberg, 1976). The hinge region is sterically unencumbered, allowing for the sulfides in the Fab' fragments to react with other chemical species (Adlersberg, 1976). The binding of Fab' fragments to TUBTS is confirmed by a decrease in the ratio of the sulfone/sulfide S_{2p} signals (Fig. 2E). Similarly, a decrease in the same ratio is observed when cysteine – an amino acid with a thiol functional group – is reacted with the TUBTS/Fab' surfaces in order to quench the remaining TUBTS molecules (Supp Info). Furthermore, a decrease in the Si_{2p} peak for the TUBTS/Fab' (3.9%) surfaces compared to the TUBTS surfaces (13.6%) is indicative of the formation of a thicker layer above the bulk quartz substrate. The N_{1s} signal for the TUBTS/Fab' surfaces rose from 0.0% to 11.2% upon binding of the Fab' fragments, confirming the presence of protein species on the surfaces.

3.2. PFP-based surfaces

Monitoring the formation of the various PFP-based surfaces was much easier due to the presence of the pentafluorophenyl group on the PFP molecules. Self-assembled monolayers of PFP were determined with the F_{1s} XPS signal increase from 0.0% (bare quartz) to 6.3%. Formation of the non-oriented Fab' and non-oriented whole antibody surfaces was monitored through the increase of the N_{1s} signal from 0.0% (PFP surfaces) to 8.8% (Fab') or 11.3% (whole antibody). Non-oriented whole antibodies or Fab' fragments bind to PFP primarily via basic amino acid side chain groups. PFP is highly specific towards amine binding, however, has also been shown to react in a small amount with thiols (Sheikh

et al., 2013). The decrease in the F_{1s} signal is indicative of the non-specific binding of the whole antibodies or Fab' fragments with the PFP surfaces. Ethanolamine was used as a blocking agent to quench the remaining PFP sites and its presence was determined by a further decrease of the F_{1s} signal to 0.0% for all surfaces involving ethanolamine.

Whole antibodies were oriented using immobilized recombinant protein G' (Fig. 2B). This protein G' is a truncated version of the original protein G lacking the albumin-binding, Fab-binding, and membrane-binding regions. Orientation of whole antibodies using protein G is a known concept and has been used by many groups in the development of assays and biosensors (Chen et al., 2011, 2013; Guo et al., 2012). Protein G has the highest affinity for human and mouse antibodies but will also bind other species – rabbit, rat, or goat (Oliver and Jamur, 2010). This is ideal as the anti-PTHrP antibodies used in this study are of mouse origin. Protein G' immobilization was verified through a decrease in the F_{1s} signal and an increase in the N_{1s} signal (Fig. 2D). As the whole antibodies are immobilized in a non-covalent arrangement with the protein G', their presence on the surfaces was confirmed by a further increase in the N_{1s} signal. Ethanolamine was used as a blocking agent to quench the remaining PFP sites and its presence was determined by a further decrease of the F_{1s} signal to 0.0% for all surfaces involving ethanolamine. However, it should be noted that ethanolamine was added after the protein G' and in order to prevent non-oriented binding of whole antibodies to the PFP groups.

3.3. Analyte and fouling signal optimization of surfaces

In order to find the most optimal surfaces for use in the biosensor, different surfaces (Fig. 3) were tested against mouse serum (surface fouling) and goat IgG (analyte signal). In this optimization stage, anti-goat IgG antibodies were used instead of anti-PTHrP antibodies due to the costly nature of the latter. Bare quartz disks exhibited a frequency shift of 30430 ± 4380 Hz against mouse serum (Fig. 3A). This extremely large value is indicative of a highly fouling surface and one that is not desirable in a biosensor. PFP and TUBTS also exhibit high levels of fouling – frequency shifts of 22050 ± 4480 Hz and 9320 ± 3420 Hz, respectively. A minimally fouling surface would exhibit serum frequency shifts of less than 5000 Hz (Sheikh et al., 2012).

In order to analyze the surfaces, a ratio of analyte signal/fouling signal was assigned to each surface (Fig. 3D). Surfaces containing non-oriented whole antibodies and Fab' fragments (Fig. 3B and C) exhibited EMPAS serum frequency shifts of ~8000–10000 Hz. Compared to PFP surfaces, there is a decrease of fouling of at least 50% due to the anti-fouling nature of proteins (Bolduc and Pelletier, 2010; Jeyachandran et al., 2010). However, analysis of the signal ratios yielded values between 0.38 and 0.44. Ethanolamine was used as a blocking agent to further decrease the fouling of the surfaces. This blocking agent has been used in the past by many groups to quench amine reactive sites on surfaces (Chen et al., 2011; Li et al., 2011). With the blocking agent, the signal ratios decreased to a range between 0.29 and 0.37. This shows that although there may have been a slight serum frequency shift decrease, there was also an analyte signal decrease. The latter is due to the fact that the analyte was binding non-specifically to the surfaces rather than to the whole antibodies/Fab' fragments.

Immobilization of whole antibodies and Fab' fragments in an oriented fashion allowed for the analyte signal to rise significantly (Fig. 3B and C). TUBTS/Oriented Fab' surfaces and PFP/Oriented Ab surfaces yielded signal ratios of 1.04 and 0.60, respectively. The serum frequency shifts for the former were 8310 ± 600 Hz and 10800 ± 1210 Hz for the latter. Although the analyte signals increased due to proper orientation of the antibodies/fragments, the fouling levels were not decreased significantly. The use of ethanolamine as a blocking agent for the PFP/Oriented Ab surfaces yielded a signal ratio of 0.95 as the analyte signal was increased, however, the fouling signal was only slightly decreased. The use of cysteine as a blocking agent had a more pronounced effect on the TUBTS/Oriented Fab' surfaces as the fouling levels were decreased to 6310 ± 80 Hz. The accompanying signal ratio of 1.26 and the serum frequency shift was still not as optimal as it could be.

Based on the previous study performed by Sheikh et al., (2013), we decided to use bovine serum albumin (BSA) as an anti-fouling agent (Fig. 3B and C). However, the surfaces were not pre-treated with the anti-fouling agent prior to the EMPAS analysis. The BSA was injected into the EMPAS flow cell before the sample injection in order to prepare the surfaces. The TUBTS/Oriented Fab' surfaces were chosen without the use of cysteine as a blocking agent due to the unnecessary redundancy of using cysteine and BSA as blocking agents. However, for the whole antibodies, it was necessary to use the PFP/Oriented Ab/ETH surfaces. In these surfaces, ethanolamine prevented the non-specific binding of whole antibodies to PFP groups. BSA proved to be a successful anti-fouling agent as serum frequency shifts were 4230 ± 40 Hz for the TUBTS/Oriented Fab' surfaces and 4410 ± 250 Hz for the PFP/Oriented Ab/ETH surfaces. This yielded signal ratios of 1.72 for the former and 2.22 for the latter. Thus, these two surfaces would be the best candidates for testing in a biosensor as they maximize analyte signal and have fouling signals less than 5000 Hz.

3.4. Calibration curves for whole antibodies and Fab' fragment biosensors

In this study whole antibody-based and Fab' fragment-based biosensors were compared. Within each group, non-mass amplified and mass-amplified biosensors were also tested (Fig. 4). Mouse monoclonal anti-PTHrP antibodies were used as the bioreecognition elements and rabbit polyclonal anti-PTHrP antibodies were used as secondary antibodies in a sandwich-type mass amplification technique. The two antibodies have different epitopes on the PTHrP protein, allowing for non-competitive binding to the protein. In order to find the linear range of the biosensors, PTHrP was injected at serially diluted concentrations (i.e. 100 μg/mL, 10 μg/mL, 1 μg/mL, etc.) until a signal was no longer detected. Once a semi-logarithmic relationship was detected, additional points were tested within the originally-tested PTHrP concentrations (i.e. 31.6 μg/mL, 3.16 μg/mL, 316 ng/mL, etc.) to illustrate the robustness of the linear range. It is important to remember that the linear ranges of the biosensors were analyzed using non-linear regressions of semi-logarithmic graphs. Various concentrations of the secondary antibody were tested against the BSA-protected whole antibody-based and Fab' fragment-based surfaces. The largest concentration (10 μg/mL) that exhibited a sub-250 Hz (noise of the EMPAS instrument) frequency shift was chosen as the concentration to be used for mass amplification.

The whole antibody-based non-mass amplified biosensor displayed a linear range from 1.85 μg/mL to 100 μg/mL and a C_{LoD} of 1.85 μg/mL (Fig. 4A). Mass amplification frequency shifts were calculated as the sum of the analyte frequency shift and the secondary antibody frequency shift. The whole antibody mass-amplified biosensor displayed a large linear range from 61 ng/mL to 100 μg/mL with a C_{LoD} of 61 ng/mL. The sensitivity of the two biosensors is shown through the comparison of the slopes of their non-linear regression lines. As expected, the mass-amplified whole antibody biosensor exhibits a higher sensitivity and lower limit of detection compared to the non-mass amplified biosensor. The biosensors in this study exhibited high reproducibility as shown by the non-linear regression analyses as well as the standard deviations of individual points on the calibration curves.

For the non-mass amplified Fab' fragment-based biosensor, a linear range from 4.96 µg/mL to 100 µg/mL and a C_{LoD} of 4.96 µg/mL was achieved. The mass-amplified Fab' fragment-based biosensor displayed a linear range from 441 ng/mL to 100 µg/mL with a C_{LoD} of 441 ng/mL (Fig. 4B). As expected, the mass-amplified biosensor exhibited a higher sensitivity and lower limit of detection compared to the non-mass amplified version. What was not expected was for the Fab' fragment-based mass-amplified biosensor to have a lower sensitivity and higher limit of detection compared to the whole antibody-based mass-amplified biosensor. Previously, some studies have found higher analyte signals when using Fab' fragments compared to whole antibodies due to a higher density of immobilized antigen-binding regions (Albers et al., 2009; Bonroy et al., 2006; Catimel et al., 1997). However, there have also been studies that have reported a decreased analyte signal for the Fab' fragments surfaces compared to the whole antibody surfaces (Peluso et al., 2003; Prisyazhnoy et al., 1988). Delair et al., (1994) reported a loss of immunological activity upon binding of the Fab' fragments to latex particles. It is possible that some of the antigen-binding regions of the Fab' fragments were compromised during the cleavage process. Mariani et al., (1991) cleaved various types of mouse IgG1 antibodies with different enzymatic methods (i.e. pepsin, ficin, bromelain, etc.) and showed that the immunological activity of the Fab' fragments ranged from 45–85% depending on the type of antibody and cleavage method used. The difficulty of optimizing the cleavage process and the actual cleavage/purification process for obtaining the Fab' fragments do not merit the potential benefits they may bring. In order to increase the analyte signal and to lower the detection limit, a better approach may be to focus on the optimization of the mass-amplification step, if possible.

The C_{LoD} of 61 ng/mL for the mass-amplified whole antibody-based biosensor was just outside the clinically-relevant range (120 pg/mL to 14 ng/mL) for PTHrP detection (Suehiro et al., 1994). Although PTHrP is an easier metastatic biomarker to detect compared to CTCs because it is present in the bloodstream at all times, the relatively low concentration range provides a challenge. Future work involves the optimization of the mass-amplification step and/or the optimization of the surface density of analyte-binding regions using various spacer ligands in order to achieve a linear range that spans the entire clinically-relevant range. Also, once the biosensor is optimized, it should be tested using serum samples as they are more representative of whole blood. The complexity of serum and the high concentrations of proteins in it will truly determine the robustness of the biosensor.

3.5. Biosensor regenerability

Whole antibody-based and Fab' fragment-based biosensors exhibited very different regenerabilities (Fig. 5). In order to test the regenerability of the biosensor, the following sequence of injections was employed: inject BSA (1.0 mg/mL), inject PTHrP (10 ug/mL), inject secondary antibody (10 ug/mL), inject 1 M glycine pH 2.0, and repeat. The glycine solution was used to remove any non-covalently bound species from the surfaces of the biosensor. The initial mass-amplified PTHrP frequency shift was taken as the relative point for the regenerability curves. It should be noted that frequency stabilization upon injection of various chemical species can vary from molecule to molecule and is dependent on the combination of factors including the mass of the adsorbed species, viscoelastic slip, non-uniform mass deposition, and rigidness of the adsorbed species (Thompson et al., 2003).

From one regeneration cycle to another, variations in the BSA (Δf_1), PTHrP (Δf_2), and secondary antibody (Δf_3) frequency shifts (Fig. 5) were observed. BSA frequency shifts did not change very much from one regeneration cycle to the next, indicating that the same amount of anti-fouling BSA was deposited on the surfaces. However, the PTHrP and secondary antibody shifts decreased from cycle to the next – although the ratio of $\Delta f_3/\Delta f_2$ was always greater than one. This shows that the analyte-binding regions were being compromised with each regeneration cycle.

The whole antibody-based biosensor displayed very poor regenerability as a result of the non-covalent interactions between the antibodies and the protein G' molecules. Since glycine washes were used to remove any non-covalently bound species, the whole antibodies were also removed from the surfaces. The PTHrP signals observed for the second to the fifth injections can be attributed solely to non-specific adsorption of the analyte. The Fab' fragment-based biosensor displayed better reproducibility, however, a loss of ~20% of the initial analyte signal intensity was observed with each subsequent glycine rinse.

4. Conclusions

In this study, we have developed the first biosensor prototype capable of detecting the breast and prostate cancer metastasis biomarker protein PTHrP. Optimization of the sensor surface – minimization of undesirable surface fouling and maximization of analyte signal – yielded two surfaces (PFP/protein G'/whole antibodies/ethanolamine and TUBTS/Fab' fragments) that required further testing in biosensing capabilities. It was determined that

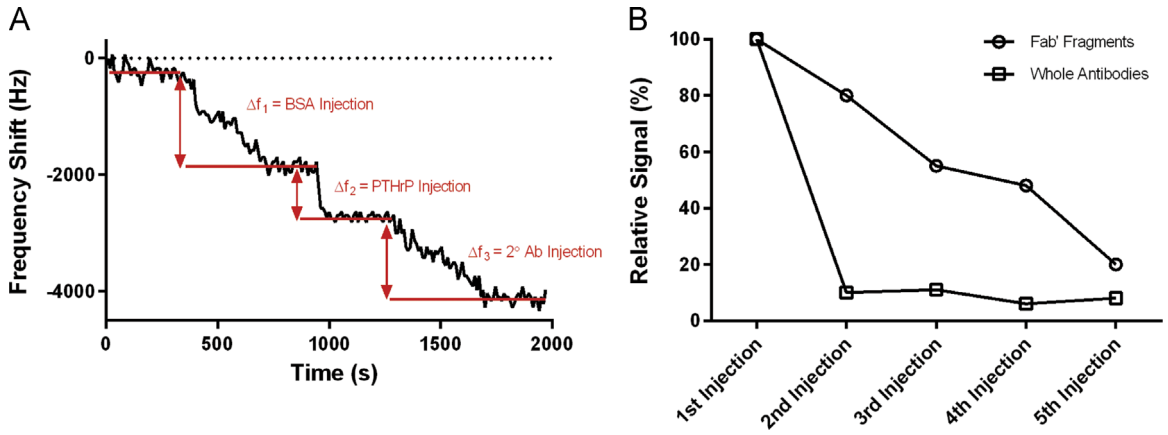

Fig. 5. (A) General EMPAS profile illustrating the frequency shifts for BSA (Δf_1), PTHrP (Δf_2), and secondary antibody (Δf_3). (B) – Regenerability curves for the whole antibody-based and Fab' fragment-based biosensors. The first mass-amplified PTHrP frequency shift is taken as a relative point for which the second to the fifth injections are compared to.

an in-line injection of bovine serum albumin prior to analyte injection provided the most minimally fouling surfaces.

Both optimized surfaces were tested as non-mass amplified and as sandwich antibody mass-amplified biosensors. The whole antibody-based mass-amplified biosensor yielded the lowest limit of detection (C_{LoD}=61 ng/mL) with the highest sensitivity and a linear range from 61 ng/mL to 100 ug/mL. It was expected that the Fab' fragment-based mass-amplified biosensor would have the lowest limit of detection, however, that was not the case (C_{LoD}=441 ng/mL). It is believed that some immunological activity was lost in the cleavage process. The Fab' fragment biosensor exhibited better regenerability compared to the whole antibody biosensor. The former showed a ~20% loss of initial analyte signal intensity after each subsequent injection, whereas the latter was only capable of detecting the analyte in the first injection. The non-covalent immobilization onto the protein G' surfaces allowed for the glycine rinses to remove the whole antibodies.

The biosensor developed in this study is the first ultra-high frequency, label-free, real-time acoustic wave sensor capable of detecting the breast and prostate cancer metastasis biomarker PTHrP. Compared to the few existing cancer metastasis biosensors, our biosensor does not rely on the detection of rare circulating tumor cells. Future work involves optimization of the mass-amplification process in order to lower the limit of detection and linear range into the clinically-relevant concentration range of PTHrP (120 pg/mL to 14 ng/mL). Once this is attained, the biosensor should be tested with serum samples containing PTHrP. Another limitation of the whole antibody-based mass-amplified biosensor is that the biorecognition elements are not bound covalently to the surface, making sensor regenerability not feasible. An alternative to oriented whole antibodies would be to use aptamers as they are highly specific towards their target analyte and can be immobilized covalently in an oriented manner more easily.

Notes

The authors declare no competing financial interest.

Acknowledgments

The authors are grateful to the National Sciences and Engineering Research Council (Grant no. RGPIN 46) for the provision of financial support. In addition, the authors wish to acknowledge Jack Sheng for his help and guidance with the EMPAS system, and Christophe Blaszykowski and Sonia Sheikh for assistance with regard to TUBTS and PFP chemistry.

Appendix A. Supplementary material

Supplementary data associated with this article can be found in the online version at http://dx.doi.org/10.1016/j.bios.2015.11.031.

References

Abdolahad, M., Sanaee, Z., Janmaleki, M., Mohajerzadeh, S., Abdollahi, M., Mehran, M., 2012. Carbon 50, 2010–2017.
Adlersberg, J.B., 1976. Ric. Clin. Lab. 6, 191–205.
Albers, W.M., Auer, S., Helle, H., Munter, T., Vikholm-Lundin, I., 2009. Colloids Surf. B 68, 193–199.
Ballantine Jr., D.S., Wohltjen, H., 1989. Anal. Chem. 61, 704A–715A.
Ballantyne, S.M., Thompson, M., 2004. Analyst 128, 1048–1055.
Benvenuto, P., Neves, M.A.D., Blaszykowski, C., Romaschin, A., Chung, T., Kim, S.R., Thompson, M., 2015. Langmuir 31, 5423–5431.
Blaszykowski, C., Sheikh, S., Benvenuto, P., Thompson, M., 2012. Langmuir. 28, 2318–2322.
Bohunicky, B., Mousa, S.A., 2011. Nanotechnol. Sci. Appl. 4, 1–10.
Bolduc, O.R., Pelletier, J.N., 2010. Anal. Chem. 82, 3699–3706.
Bonroy, K., Frederix, F., Reekmans, G., Dewolf, E., De Palma, R., Borghs, G., Declerck, P., Goddeeris, B., 2006. J. Immunol. Methods 312, 167–181.
Catimel, B., Nerrie, M., Lee, F.T., Scott, A.M., Ritter, G., Welt, S., Old, L.J., Burgess, A.W., Nice, E.C., 1997. J. Chromatogr. A 776, 15–30.
Chen, J.-C., Sadhasivam, S., Lin, F.-H., 2011. Process Biochem. 46, 543–550.
Chen, J.K., Zhou, G.Y., Chang, C.J., 2013. Sens. Actuators B Chem. 186, 802–810.
Costa, C., Abal, M., López-López, R., Muinelo-Romay, L., 2014. Sensors 14, 4856–4875.
Crivianu-Gaita, V., Romaschin, A., Thompson, M., 2015. Biochem. Biophys. Rep. 2, 23–28.
Crivianu-Gaita, V., Thompson, M., 2015. Biosens. Bioelectron. 70, 167–180.
Delair, T., Pichot, C., Mandrand, B., 1994. Colloid Polym. Sci. 272, 72–81.
Geiger, T.R., Peeper, D.S., 2009. Biochim. Biophys. Acta Rev. Cancer 1796, 293–308.
Guise, T.A., Yin, J.J., Taylor, S.D., Kumagai, Y., Dallas, M., Boyce, B.F., Yoneda, T., Mundy, G.R., 1996. J. Clin. Invest. 98, 1544–1549.
Guo, S.L., Chen, P.C., Chen, M.S., Cheng, Y.C., Lin, J.M., Lee, H.C., Chen, C.S., 2012. Plos One 7, 1–8.
Hader, A., Achik, I., Hajjaji, A., Boughaleb, Y., 2012. Opt. Mater. 34, 1713–1716.
Hall, W.A., Djalilian, H.R., Nussbaum, E.S., Cho, K.H., 2000. Med. Oncol. 17, 279–286.
Jeyachandran, Y.L., Mielczarski, J.A., Mielczarski, E., Rai, B., 2010. J. Colloid Interface Sci. 341, 136–142.
Kaspar, M., Stadler, H., Weib, T., Ziegler, Ch, 2000. Fresenius J. Anal. Chem. 366, 602–610.
Li, D., Wang, J., Wang, R., Li, Y., Abi-Ghanem, D., Berghman, L., Hargis, B., Lu, H., 2011. Biosens. Bioelectron. 26, 4146–4154.
Liu, H., May, K., 2012. MAbs 4, 17–23.
Lyden, D., Welch, D.-R., Psaila, B., 2011. Cancer Metastasis: Biologic Basis and Therapeutics, first ed. Cambridge University Press, New York.
Mariani, M., Camagna, M., Tarditi, L., Seccamani, E., 1991. Mol. Immunol. 28, 69–77.
Morisot, A., Bessaoud, F., Landais, P., Rebillard, X., Tretarre, B., Daures, J.-P., 2015. Med. Res. Methodol. 15, 1–14.
Mundy, G.R., Edwards, J.R., 2008. J. Am. Soc. Nephrol. 19, 672–675.
Nakajima, T., Konda, Y., Kanai, M., Izumi, Y., Kanda, N., Nanakin, A., Kitazawa, S., Chiba, T., 2002. Dig. Dis. Sci. 47, 2729–2737.
Neves, M.A.D., Blaszykowski, C., Bokhari, S., Thompson, M., 2015. Biosens. Bioelectron. 72, 383–392.
Nishihara, M., Kanematsu, T., Taguchi, T., Razzaque, M.S., 2007. Ann. N. Y. Acad. Sci. 1117, 385–392.
Oliver, C., Jamur, M.-C., 2010. Immunocytochemical Methods and Protocols, third ed. Springer, London.
Peluso, P., Wilson, D.S., Do, D., Tran, H., Venkatasubbaiah, M., Quincy, D., Heidecker, B., Poindexter, K., Tolani, N., Phelan, M., Witte, K., Jung, L.S., Wagner, P., Nock, S., 2003. Anal. Biochem. 312, 113–124.
Prisyazhnoy, V.S., Fusek, M., Alakhov, Y.B., 1988. J. Chromatogr. 424, 243–253.
Schreiber, F., 2000. Prog. Surf. Sci. 65, 151–256.
Sheikh, S., Blaszykowski, C., Thompson, M., 2013. Surf. Interface Anal. 45, 1781–1784.
Sheikh, S., Blaszykowski, C., Thompson, M., 2011. Talanta 85, 816–819.
Sheikh, S., Yang, D.Y., Blaszykowski, C., Thompson, M., 2012. Chem. Commun. 48, 1305–1307.
Suehiro, M., Murakami, M., Fukuchi, M., 1994. Ann. Nucl. Med. 8, 231–237.
Thompson, M., Ballantyne, S.M., Cheran, L.-E., Stevenson, A.C., Lowe, C.R., 2003. Analyst 128, 1048–1055.
Thompson, M., Blaszykowski, C., Sheikh, S., Romaschin, A., 2014. Biosens. Bioelectron. 67, 3–10.
Viitala, T., Vikholm, I., Peltonen, J., 2000. Langmuir 16, 4953–4961.
Vikholm-Lundin, I., 2005. Langmuir 21, 6473–6477.
Vikholm-Lundin, I., Albers, W.M., 2006. Biosens. Bioelectron. 21, 1141–1148.
Weber, G.F., 2008. Cancer Lett. 270, 181–190.
Weigelt, B., Peterse, J.-L., van't Veer, L.-J., 2005. Nat. Rev. 5, 591–602.
Wilson, D.S., Wu, J., Peluso, P., Nock, S., 2002. Reactions 260, 29–36.